

# Simultaneous removal of organic micropollutants and inorganic heavy metals by nano-calcium peroxide induced Fenton-like treatment

Hui Xia<sup>a,b</sup>, Tao Lyu<sup>c</sup>, Jungang Guo<sup>a,b,\*</sup>, Chuanqi Zhao<sup>d,\*</sup>, Yuesuo Yang<sup>e,\*</sup>

<sup>a</sup> Zhengzhou Institute of Multipurpose Utilization of Mineral Resources, CAGS, Zhengzhou 450006, China;

<sup>b</sup> China National Engineering Research Center for Utilization of Industrial Minerals, Zhengzhou 450006, China;

<sup>c</sup> School of Water, Energy and Environment, Cranfield University, College Road, Cranfield, Bedfordshire, MK43 0AL, United Kingdom;

<sup>d</sup> School of Materials and Environment, Guangxi University for Nationalities, Nanning 530006, China;

<sup>e</sup> Key Lab of Groundwater Resources and Environment (Jilin University), Ministry of Education, Changchun 130021, China.

Corresponding authors: gjg801@163.com (J.G.); zcqs@aliyun.com (C.Z.); yangyuesuo@jlu.edu.cn (Y.Y.).

## Abstract

Groundwater can be contaminated by both organic micropollutants and inorganic heavy metals and thus, it is essential to develop environmental-friendly and cost-effective technologies for the remediation of such multiple contaminants. Advanced nanomaterials, including nano-calcium peroxide (nano-CaO<sub>2</sub>), induced Fenton-like treatment has been recently developed to effectively oxidise and remediate various organic micropollutants. The Ca(OH)<sub>2</sub> residues have the potential to further remove toxic heavy metals via precipitation, however, it has been rarely studied. To investigate the proposed feasibility and understand the mechanisms, an optimised pH-regulated chemical precipitation method was developed to synthesis the nano-CaO<sub>2</sub> material and then catalysed by Fe(II) towards Simultaneous removal of the model compounds of *p*-nitrophenol (PNP) and cadmium (Cd). The Electron Spin Resonance (ESR) measurements demonstrated that hydroxyl radicals ( $\cdot\text{OH}$ ) and singlet oxygen ( $^1\text{O}_2$ ) are two major reactive oxygen species that lead to 93% removal of PNP (40 mg/L), and simultaneously, over 99% of the Cd (10 mg/L) was removed through the precipitation with Ca(OH)<sub>2</sub> and/or co-precipitation with ferrite using optimum conditions (Fe<sup>2+</sup> = 75 mg/L, nano-CaO<sub>2</sub> = 500 mg/L, pH<sub>ini</sub> = 2.8, oscillation frequency = 160 rpm, T = 298 K). The existence of sunlight illumination and competition ions, i.e. K<sup>+</sup>, Na<sup>+</sup>, Ca<sup>2+</sup>, Mg<sup>2+</sup>, SO<sub>4</sub><sup>2-</sup>, NO<sub>3</sub><sup>-</sup>, and Cl<sup>-</sup>, showed negligible effect on the removal performance, which supported its feasibility for the treatment of both ground- and surface water. Nevertheless, some environmental conditions, such as pH, temperature, HCO<sub>3</sub><sup>-</sup> and Mn<sup>2+</sup> should be taken into consideration during the application as they could led obvious impacts on the treatment. Overall, this study provided a new groundwater ex-situ remediation technology that removed organic micropollutants and inorganic heavy metals simultaneously via mechanisms revealed nano-remediation technique.

**Keywords:** advanced oxidation process; co-precipitation; groundwater treatment; nano-

remediation technology; reactive oxygen species

## 1. Introduction

Groundwater is an essential freshwater resource, on which the survival and development of the whole ecosystem depend, including human populations [1-3]. However, the continual increase in industrial and agricultural activities has resulted in a gradual decline in the environmental quality of groundwater, with groundwater environments becoming increasingly contaminated with anthropogenic pollutants such as organic micropollutants, such as pharmaceuticals and personal care products (PPCPs), endocrine-disrupting chemicals (EDCs)[4], and inorganic heavy metals, such as arsenate (As), chromium (Cr), and cadmium (Cd)[5-7].

As a typical nitroaromatic pollutant in groundwater, *p*-nitrophenol (PNP) has been widely used in agriculture, dyes/pigments, engineering polymers and pharmaceuticals[8]. After the inappropriate discharge and pre-treatment, PNP can seep and penetrate the soil layer under the action of environmental forces and present in groundwater [9]. Even at the low exposure level ( $LD_{50}=250$  mg/kg, rats orally) [10], PNP can cause eye and skin irritation, methemoglobinemia, cyanosis, coma and other health effects [11, 12]. Heavy metals such as cadmium (Cd) in groundwater is often considered an environmentally hazardous substance, which can result in kidney disease, bone disease, lung function damage, cell cancer or death in severe cases [13, 14]. Moreover, both aforementioned compounds are chemically stable, not easily degraded under natural conditions and bioaccumulated in the environment, thus presenting a long-term risk to groundwater systems [10, 15]. Therefore, it is essential to develop environmental-friendly and cost-effective technologies for the remediation of such multiple contaminants.

Advanced nano-remediation techniques have developed rapidly, achieving good results in the field of groundwater pollution remediation [16-18]. For example, nano-zero-valent iron, graphene oxide, iron sulphide nanoparticles and nanoscale magnesium peroxide have been used to remove trichloroethylene [19], Cd [20], hexavalent chromium [21] and toluene [22] from groundwater, respectively. Recently, nano-calcium peroxide (nano- $CaO_2$ ) has drawn high attention due to its multi-functionality, high efficiency, and environmental friendliness (Table 1). Nano- $CaO_2$  contains a high-energy peroxide covalent bond (-O-O-) in its chemical structure which has high oxidation activity (Fig. S1), undergoing deliquescence in aqueous environments (as described in Eq. 1 and Eq. 2). The  $O_2$ ,  $H_2O_2$  and  $Ca(OH)_2$  released during nano- $CaO_2$  hydrolysis have previously been applied to facilitate the bio-remediation, chemical-remediation and physical-remediation processes [23].





The recent development and application of Nano-CaO<sub>2</sub> for environmental remediation are summarized in Table 1. It can be found that Nano-CaO<sub>2</sub> has been successfully used for the removal of organic pollutants. Qian et al. synthesized nano-CaO<sub>2</sub> for the degradation of toluene, showing that toluene degradation was removed completely in 3 days[24]. Sun et al. used nano-CaO<sub>2</sub>/Fe<sup>2+</sup> to degrade trichloroethylene in groundwater, confirming that nano-CaO<sub>2</sub> could achieve a higher removal rate (70.4% vs. 61.1%) than traditional CaO<sub>2</sub> under the same conditions [25], and the nano-CaO<sub>2</sub> performed better than commercial CaO<sub>2</sub> in naphthalene removal (84.5% vs. 95.4%) when catalyzed by Fe(II)/citric acid[26]. Moreover, nano-CaO<sub>2</sub> has been definitely confirmed to have obvious broad-spectrum reactivity in the removal of more organic pollutants such as polycyclic aromatic hydrocarbons, benzene series, and chlorinated hydrocarbon[27]. In addition, nano-CaO<sub>2</sub> has been used as a filling material in a groundwater permeable reaction barrier system, providing an oxygen source for microorganisms and therefore, supporting effective bioremediation [28]. The reactions were mainly based on either the first hydrolysate of H<sub>2</sub>O<sub>2</sub> or the second hydrolysate of O<sub>2</sub>. Some studies have also investigated the possibilities of using nano-CaO<sub>2</sub> for the treatment of inorganic pollutants, such as arsenic, phosphorus and silver, via chemical precipitation[28-30]. Nevertheless, those experiments were conducted separately only for a single pollution type, but did not carry out co-remediation of organic and inorganic combined pollution. We claim that the third hydrolysate of Ca(OH)<sub>2</sub> could further contribute to the remove of inorganic heavy metals, which may pave a way to simultaneously removal organic micropollutants and inorganic heavy metals. To be sure, the synthesis process of nano-CaO<sub>2</sub> was slightly improved, and it is novel to propose an intermediate CaCl<sub>2</sub>·8NH<sub>3</sub> that would be favourable for the diffusion of nanoparticles.

Herein, a nano-CaO<sub>2</sub>/Fe<sup>2+</sup> catalytic technique was established to systematically study the simultaneous remediation of PNP and Cd, as the model organic micropollutant and toxic heavy metal respectively. The optimum dose ratio of nano-CaO<sub>2</sub> and Fe<sup>2+</sup> were studied to achieve the best removal efficiencies of both PNP and Cd. Besides, electron spin resonance (ESR) technology and free radical quenching experiments were conducted to reveal key reactive oxygen species (ROs) that contribute to PNP degradation. The effects of the existence of common anions and cations, i.e. Na<sup>+</sup>, K<sup>+</sup>, Ca<sup>2+</sup>, Mg<sup>2+</sup>, Fe<sup>3+</sup>, Mn<sup>2+</sup>, HCO<sub>3</sub><sup>-</sup>, SO<sub>4</sub><sup>2-</sup>, Cl<sup>-</sup>, and NO<sub>3</sub><sup>-</sup>, were also investigated to indicate the real-world implementation feasibility. Additionally, the treatment processes were also evaluated under different simulated environmental conditions, such as various initial pH, oscillation frequency (water movement), temperature and light illumination. With these results, the feasibility of practical application of this technology for the simultaneously remediation of organic micropollutants and heavy metals was discussed.

**Table 1**Summary of nano-CaO<sub>2</sub> synthesis and application in environmental remediation

Main materials	Particle size	Contaminants (concentration)	Removal mechanism	Maximum removal rate or	Year	Reference
CaCl <sub>2</sub> , H <sub>2</sub> O <sub>2</sub> , PEG 200	125 nm	Naphthalene (0.1 mM)	Chem-oxidation	Over 99% (180 min)	2022	[27]
	125 nm	Naphthalene (0.1 mM)	Chem-oxidation	95.4% (180 min)	2021	[26]
	50-200 nm	Trichloroethylene (1.5 mM)	Chem-oxidation	Over 70.4% (180 min)	2019	[25]
	109 nm	BTEX (0.5 mM)	Chem-oxidation	Over 90% (180 min)	2019	[25]
	No given	Acrylic acid (2882–7206 mg/L)	Physisorption	Almost 100% (140 min)	2018	[31]
	5-15 nm	α-toluic acid (7.06 g/L)	Physisorption	98.05% (34 min)	2017	[32]
	10-40 nm	Benzeneacetic acid (6.8 g/L)	Physisorption	94.49% (30 min)	2017	[33]
	5-15 nm	α-toluic acid (5446 mg/L)	Physisorption	4697.2 mg/g	2016	[34]
	15-25 nm	Arsenic (0.4 mg/L)	Chem-precipitation	Over 88% (30 min)	2012	[35]
15-25 nm	Silver nanoparticles (No given)	Chem-oxidation	Over 90% (8 hours)	2011	[29]	
CaCl <sub>2</sub> , H <sub>2</sub> O <sub>2</sub> , CTAB <sup>a</sup>	No given	Diclofenac sodium (0.02 mM)	Chem-oxidation	97.5% (180 min)	2021	[36]
CaCl <sub>2</sub> , H <sub>2</sub> O <sub>2</sub> , PVA <sup>b</sup>	14-19 NM	Trichloroethylene (0.15 mM)	Chem-oxidation	91% (360 min)	2020	[37]
	13-62 nm	Benzene (50 mg/L)	Bio-remediation	100% (90 days)	2019	[38]
CaSO <sub>4</sub> , H <sub>2</sub> O <sub>2</sub>	No given	Naphthalene (20 mg/L)	Bio-remediation	100% (50 days)	2018	[28]
	13-62 nm	Benzene (50 mg/L)	Bio-remediation	100% (60 days)	2017	[39]
Ca(NO <sub>3</sub> ) <sub>2</sub> , H <sub>2</sub> O <sub>2</sub>	20-50 nm	Methyl blue (0.01 mM)	Photo-oxidation	Over 80% (80-100 min)	2016	[40]
Nano-Ca(OH) <sub>2</sub> , H <sub>2</sub> O <sub>2</sub>	100-200 nm	Toluene (0.2-0.6 mM)	Chem-oxidation	100% (3 days)	2013	[24]
Common CaO <sub>2</sub> (Grind)	110 nm	Diesel (1000 mg/L)	Bio-remediation	60% (14 days)	2018	[41]
Biochar, CaCl <sub>2</sub> , H <sub>2</sub> O <sub>2</sub> , PEG 200	20-25 nm	PO <sub>4</sub> <sup>3-</sup> (100 mg/L)	Chem-precipitation,	213.22±13.57 mg/g	2020	[30]

<sup>a</sup>: CTAB - Cetyltrimethylammonium bromide; <sup>b</sup>: PVA - Polyvinyl alcohol.

## 2. Materials and methods

### 2.1. Materials

The chemicals of *P*-nitrophenol (Cas: 100-02-7, Shanghai Maclean Biochemical Technology Co. Ltd., Shanghai, China), CaO<sub>2</sub> (70%, Cas: 1305-79-9, Shandong Xiya Chemical Industry Co. Ltd., Shanghai, China), FeSO<sub>4</sub>•7H<sub>2</sub>O (Cas: 7782-63-0, Xilong Chemical Co. Ltd., Guangdong, China), FeCl<sub>3</sub>•6H<sub>2</sub>O (Cas: 10025-77-1, Tianjin Damao Chemical Reagent Factory, Tianjin, China), were obtained from Tianjin Bodi Chemical Co. Ltd., Tianjin, China. Other reagents, such as CdSO<sub>4</sub> (≥99.0%, Cas: 7790-84-3), H<sub>2</sub>O<sub>2</sub> (30%, Cas: 7722-84-1), CdSO<sub>4</sub> (Cas: 7790-84-3), 5,5-Dimethyl-1-pyrroline-N-oxide (DMPO, 97.0%, Cas: 3317-61-1) and 2,2,6,6-tetramethylpiperidine oxidation (TEMPO, 97.0%, Cas: 2564-83-2), were purchased from Sinopharm Chemical Reagent Co. Ltd., Shanghai, China. All reagents were of analytical grade or higher.

### 2.2. Preparation of nano-CaO<sub>2</sub>

The synthesis of nano-CaO<sub>2</sub> was performed based on a modified version of the method from [40], in which CaCl<sub>2</sub> was used as the precursor rather than Ca(NO<sub>3</sub>)<sub>2</sub> as it is more economical and the sequence of addition of H<sub>2</sub>O<sub>2</sub> and NH<sub>3</sub>•H<sub>2</sub>O was changed. The specific process was as follows: (i) First, 11.1 g of CaCl<sub>2</sub> was weighed and transferred to a 200 mL beaker, combined with 25 mL of pure water and dissolved with ultrasonication (40 KHz, 10-20 min). It is of note, that as CaCl<sub>2</sub> is hydrolyzed to produce slightly soluble Ca(OH)<sub>2</sub>, its aqueous solution will become cloudy for a while. (ii) Once dissolved, 35 mL of NH<sub>3</sub>•H<sub>2</sub>O was added to the solution, followed by 20 mL of 30% H<sub>2</sub>O<sub>2</sub>, which was then slowly injected into the solution at 0.2 mL/min, with mixing maintained at 500 rpm throughout the whole process. A yellowish CaO<sub>2</sub> precipitation was gradually formed and increased with ongoing injection of H<sub>2</sub>O<sub>2</sub>; (iii) The precipitation was then centrifuged at the high speed of 11000 rpm for 20 min, then washed three times with pure water and ethanol, sequentially, then dried at 80 °C for more than 2 hours.

### 2.3. Characterization of nano-CaO<sub>2</sub>

The morphological features and particle size of synthetic nano-CaO<sub>2</sub> particle samples were measured by scanning electron microscope (SEM, SIGMA500, Zeiss, Germany) and transmission electron microscope (TEM, TECNAIG2F20-S-TWIN, FEI, UK). It is of note, that the samples were pre-processed using a gold spray to achieve a high-definition SEM image, with a small number of samples ultrasonically dispersed in an ethanol solution for 5 min prior to TEM scanning. X-ray diffraction (XRD, D/max-2500PC, Rigaku, Japan) was conducted to identify the crystallographic structure of samples using a computer-controlled X-ray diffractometer. Raman spectrometry (HR Evolution, Varian, Germany), X-ray photoelectron spectroscopy (XPS, AXIS

Supra, Kratos, UK) and Fourier transform infrared spectroscopy (FTIR, Nicolet iS5, Thermo, USA) were used to identify the molecular structure of the peroxide covalent bond in nano-CaO<sub>2</sub>.

#### 2.4. Experimental Procedures

200 mL of synthetic 40 mg/L PNP and 10 mg/L Cd multiple solution with controlled pH<sub>ini</sub> was combined in a 250 mL conical bottle. Different pH<sub>ini</sub> (2.6, 2.8, 5.0, 7.0, 9.0, 11.0) was adjusted using 0.01 – 0.1 M HCl/NaOH to evaluate the effect of pH changes on the mix-pollution remediation. Then, different dosage of Fe<sup>2+</sup> (0, 5, 10, 15, 20 mg) and nano-CaO<sub>2</sub> (0, 50, 75, 100, 125 mg) were added successively for optimal material consumption. The degradation experiment was performed immediately using a constant temperature oscillator at OF=160 rpm and T=298 K. 3 mL samples were taken at 30, 60, 120 and 180 min, respectively, with each sample filtered through a 0.22 μm water filtration membrane. From each collected sample, 2 mL was used for PNP determination and 1 mL was used for Cd measurements. The effect of sampling volume was ignored. Each treatment was carried out in triplicate.

In addition, batch investigations were performed under simulated groundwater environment conditions including in hydrochemical characteristics, no light exposure, temperature, fluctuation. The hydrochemical characteristics of groundwater were simulated by adjusting the pH<sub>ini</sub>, and using predetermined concentrations of the various ions (NaHCO<sub>3</sub> = 688 mg/L, MgSO<sub>4</sub> = 996 mg/L, CaCl<sub>2</sub> = 555 mg/L, NaSO<sub>4</sub> = 309 mg/L, KNO<sub>3</sub> = 326 mg/L, MnSO<sub>4</sub> = 272 mg/L, Fe<sub>2</sub>(SO<sub>4</sub>)<sub>3</sub> = 360 mg/L) while changing only one of factor at a time. And additional control experiments with dark (no light exposure), relatively high temperature (323 K) and low oscillation frequency (60 rpm) were performed, respectively. Worthy of note was that variations in the movement of the groundwater were simulated by changing the oscillation frequency so as to investigate the serviceability in an underground environment.

#### 2.5. Analytical methods

PNP was determined by UV-Vis spectrophotometry (U-2910, Hitachi, Japan) [9]. Firstly, in order to terminate the degradation reaction, 2 mL of the sample was immediately mixed with 1 mL excess methanol to quench ·OH; Secondly, the sample was acidified by adding HCl (1 mL, 50% V/V) and heating the mixture at 60 °C for 20 min to eliminate interference from fine particles such as Fe(OH)<sub>3</sub>, Ca(OH)<sub>2</sub> and Cd(OH)<sub>2</sub>. Thirdly, ascorbic acid (1 mL, 5 g/L) was added immediately after cooling to eliminate the colour of trivalent iron. Finally, the final colorimetric volume was fixed to 10 mL, and colorimetric determination of PNP was performed at 317 nm, exhibiting the ultraviolet characteristic peak of PNP under acidic conditions.

Cd was determined by flame atomic absorption spectrophotometry (SpectrAA 220 with GTA 110, Varian, Germany). Fe was determined using inductively coupled plasma emission spectrometry (ICPE-9000, Shimadzu, Japan). Details pertaining to the quantitative analytical

methods used for H<sub>2</sub>O<sub>2</sub> and CaO<sub>2</sub>, as well as the qualitative analytical method for ROS, are provided in the *Supporting Materials*.

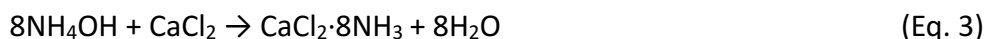
### 3. Results and discussion

#### 3.1. Characterization of the nano-CaO<sub>2</sub>

Nano-CaO<sub>2</sub> and the CaO<sub>2</sub> commercial reagent were subjected to XRD and Raman spectroscopy, with the results shown in Fig. 1A and Fig. 1B, respectively. Based on the XRD pattern, the phase and intensity of the major observed peaks were attributed to CaO<sub>2</sub> (d = 3.058, 2.961, 2.524 and 1.916; JCPDS card number 85-0514; see (a) in Fig. 1A). However, there were also some minor peaks for CaClOH observed (d = 4.947, 3.177, 2.352 and 1.916; JCPDS card number 73-1885; see (b) in Fig. 1A), the occurrence of which depended on the conditions of synthesis. Titration of the synthetic material with KMnO<sub>4</sub> showed that the CaO<sub>2</sub> content was about 71%, which was consistent with the XRD results. The Raman spectra of the synthesized nano-CaO<sub>2</sub> and the CaO<sub>2</sub> reagents (Fig. 1B) exhibited a distinct characteristic peak at 835 cm<sup>-1</sup> [42], and the XPS peak at 531.0 eV (Fig. 1D) and the FTIR absorption peak at 875 cm<sup>-1</sup> (Fig. 1E) observed for nano-CaO<sub>2</sub>, were similar to those of CaO<sub>2</sub> as reported in the literature, which was attributed to the peroxide bond (-O-O-) of CaO<sub>2</sub> [30, 43, 44].

The SEM image in Fig. 1C showed that the morphology of a single particle of synthesized nano-CaO<sub>2</sub> was approximately a sphere with a particle diameter of about 46 nm. The particle size established by SEM analysis was consistent with the results of TEM imaging (Fig. 1F). However, the shape of a single particle size was found to be similar to the symbol 8 in TEM images (Fig. S2), which might be related to the chemical structure of CaO<sub>2</sub> (Fig. S1). Overall, the results of XRD, RAMAN, XPS, FTIR, SEM and TEM analysis confirm that the synthesized material was CaO<sub>2</sub> nanoparticles.

The mechanism of nano-CaO<sub>2</sub> synthesis can be summarised as follows. The complex CaCl<sub>2</sub>·8NH<sub>3</sub> was formed from CaCl<sub>2</sub> in a high concentration ammonia solution according to the reaction described in Equation 3. It is worth noting that the CaCl<sub>2</sub> solution would be cloudy due to the inhalation of CO<sub>2</sub> in the air. Once the high concentration ammonia was added, the solution would immediately become clear and translucent. The existence of CaCl<sub>2</sub>·8NH<sub>3</sub>, thus, could be confirmed. The main product CaO<sub>2</sub> was formed from the reaction between H<sub>2</sub>O<sub>2</sub> and CaCl<sub>2</sub>·8NH<sub>3</sub>, along with the by-products HCl and NH<sub>4</sub>OH (Eq. 4), with these by-products undergoing an acid-base neutralization reaction (Eq. 5), which further promoted the formation of CaO<sub>2</sub>.



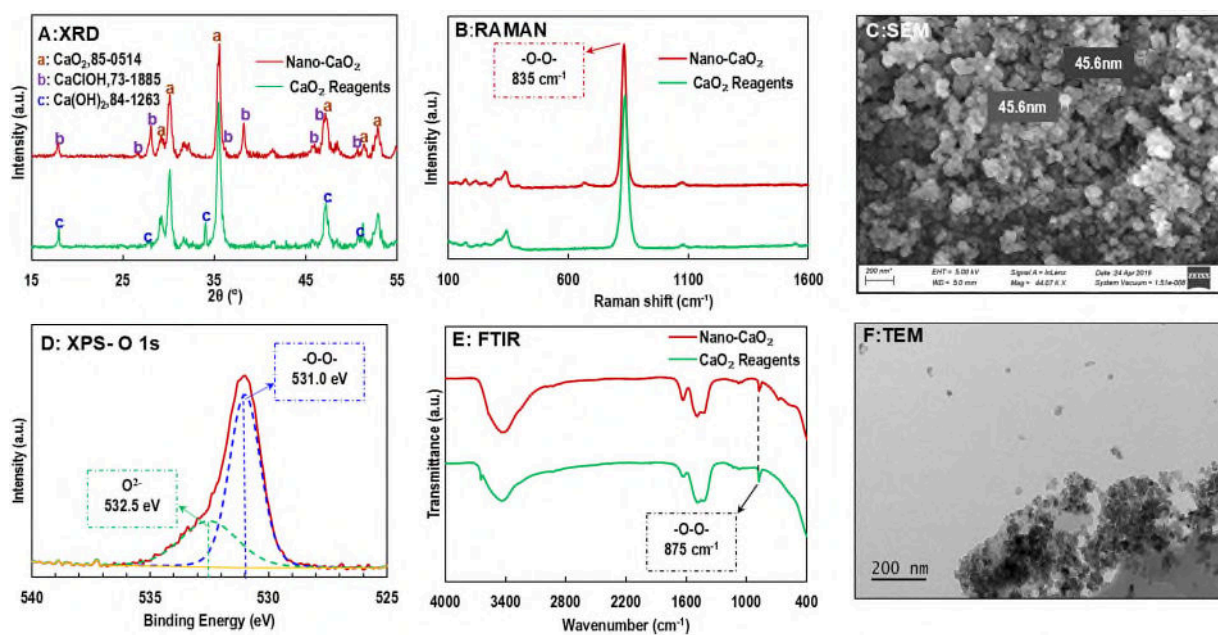


**Figure 1.** Characterization of nano-CaO<sub>2</sub>: A) XRD spectra; B) Raman spectra; C) SEM image; D) TEM image; E) XPS O 1s spectra; F) FTIR spectra.

### 3.2. The improvement of the nano-CaO<sub>2</sub> synthesising

As outlined in Table 1, there are four current methods for the synthesis of nano-CaO<sub>2</sub>: (i) Using CaCl<sub>2</sub> as a precursor, NH<sub>3</sub>·H<sub>2</sub>O is added initially to neutralize the by-product HCl, followed by the slow dropwise addition of H<sub>2</sub>O<sub>2</sub> and polymers (PEG-200/PVA) under high-speed stirring conditions [29, 31, 33-35, 37, 43, 45]. (ii) The Ca(NO<sub>3</sub>)<sub>2</sub> precursor is mixed directly with H<sub>2</sub>O<sub>2</sub> and then adjusted to a strong alkaline pH using NH<sub>3</sub>·H<sub>2</sub>O or NaOH, while maintaining high-speed stirring throughout the synthesis process [40]. (iii) Using a CaSO<sub>4</sub> emulsion as a precursor, an excess of KOH and H<sub>2</sub>O<sub>2</sub> were injected into the emulsion under high-speed stirring conditions [28, 38, 39, 46]. (iv) Using CaO<sub>2</sub> as a raw material, nano-CaO<sub>2</sub> is prepared by high-speed rapid physical grinding [41].

Compared with the aforementioned existing methods for nano-CaO<sub>2</sub> synthesis, the optimized synthesis method used in the present study had the advantages of generating high purity of products, with large volumes formed, at low cost and with easy separation, making the optimized method suitable for engineering applications. Using the optimized method separation was easier to perform than synthesis method (i), avoiding the need to add the polymer PEG-200. Compared with method (ii), adjusting the sequence of addition of NH<sub>3</sub>·H<sub>2</sub>O and H<sub>2</sub>O<sub>2</sub>, resulted in the nanoparticles being more dispersed due to the formation of intermediate complex CaO<sub>2</sub>·8NH<sub>3</sub>, while also avoiding the need to use a controlled nitric acid reagent. Using the optimized method, the amount of nano-CaO<sub>2</sub> synthesized was larger than

using method (iii), with the purity of products also being higher. Furthermore, the particle size of nanoparticles was about 46 nm, which was smaller than that of method (iv) while a particle diameter of 110 nm was produced using the fourth method of physical grinding.

### 3.3. Removal performance of PNP and Cd and associated mechanisms

#### 3.3.1. PNP removal

A Fenton-like advanced oxidation process can be performed using  $\text{Fe}^{2+}$  as a catalyst to hydrolyse  $\text{H}_2\text{O}_2$  from  $\text{CaO}_2$ , for use in the oxidative degradation and removal of organic pollutants [47]. Furthermore, a  $\text{Ca}(\text{OH})_2$  hydrolysate from  $\text{CaO}_2$  can be used for the precipitation and removal of heavy metals [48, 49]. Based on these two principles, nano- $\text{CaO}_2$  was designed and synthesized to treat the co-existing pollutants PNP and Cd, with the results shown in Fig. 2. The removal rates of PNP and Cd reached 93% and 99% in 180 min, respectively (Fig. 2 A, blue arrow), indicating that nano- $\text{CaO}_2$  could effectively remove both organic compounds and heavy metals.

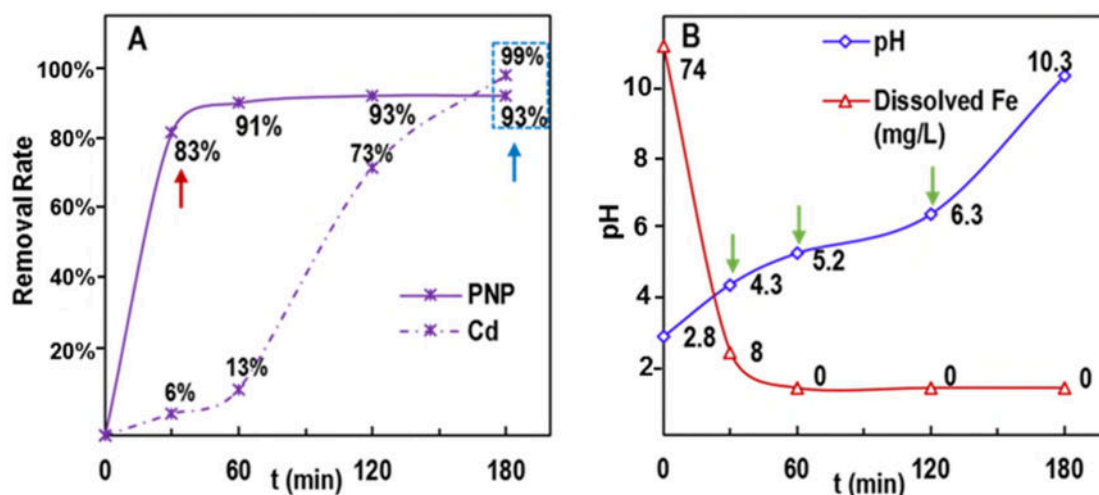
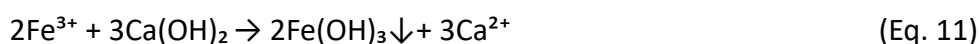


**Figure 2.** Performance in the removal of PNP and Cd. The solid line represents the PNP data and the dashed line represents the Cd data. Experimental conditions: solution volume = 200 mL, initial PNP = 40 mg/L, initial Cd = 10 mg/L,  $\text{Fe}^{2+}$  = 75 mg/L, nano- $\text{CaO}_2$  = 500 mg/L,  $\text{pH}_{\text{ini}}$  = 2.8, oscillation frequency = 160 rpm,  $T$  = 298 K.

As shown in Fig. 2A, the degradation and removal efficiency of PNP reached 83% within 30 min (Fig. 2A, red arrow). This indicates that the PNP degradation process mainly occurred in the initial stage of the reaction, as  $\text{CaO}_2$  is catalyzed by  $\text{Fe}^{2+}$  to rapidly produce highly active  $\cdot\text{OH}$ , which can degrade PNP under acidic conditions in the first 30 min of the reaction. The catalytic degradation mechanism was as follows: Firstly,  $\text{CaO}_2$  preferentially reacted with  $\text{H}^+$ , rapidly forming  $\text{H}_2\text{O}_2$  under acidic conditions (Eq. 7). Secondly,  $\text{H}_2\text{O}_2$  was catalyzed by  $\text{Fe}^{2+}$  to form  $\cdot\text{OH}$  (Eq. 8) and finally, PNP was degraded by  $\cdot\text{OH}$  (Eq. 9) [50-52]. Detailed analysis of the PNP degradation process showed that there was a large amount of dissolved iron present in the

solution, with degradation occurring rapidly in the first 30 min, while dissolved iron was not detected in the system after 60 min, at which point PNP degradation was negligible. The PNP degradation curve is shown in Fig. 2A, and the dissolved iron concentration curve is shown in Fig. 2B, exhibiting an opposite trend to that of PNP degradation, indicating that PNP degradation was closely affected by dissolved iron and therefore, confirmed the catalytic mechanism.  $\text{Ca(OH)}_2$ , one of the hydrolyzed products of  $\text{CaO}_2$ , increased the pH of the system (see the blue line in Fig. 2B), causing  $\text{Fe}^{2+}$  and  $\text{Fe}^{3+}$  to precipitate with  $\text{OH}^-$  (Eq. 10 and Eq. 11), depleting dissolved iron and resulting in PNP degradation ceasing due to the absence of available catalysts.



### 3.3.2. Role of ROSs

In order to verify the mechanism of PNP degradation by nano- $\text{CaO}_2/\text{Fe}^{2+}$ , the  $\cdot\text{OH}$  capture agent DMPO and the  $^1\text{O}_2$  capture agent TEMPO were added to different systems for ROSs analysis by ESR respectively, as shown in Fig. 3A and Fig. 3B. The 1:2:2:1 pattern in Fig. 3A demonstrated the presence of  $\cdot\text{OH}$  [53]. However, it was found that under acidic conditions the  $\cdot\text{OH}$  peak height was smaller than in the non-acidic system (Fig. 3A), which contradicts the established theory that the Fenton-like process had a higher reaction activity under acidic conditions. The observed colour changes in the system (solution became faint pink when the acid was added) indicated that other chemical changes occurred during the capture process, resulting in a decrease in the  $\cdot\text{OH}$  peak shape.

Moreover, the presence of  $^1\text{O}_2$  was confirmed by the 1:1:1 peak in Fig. 3B [54]. In the process of  $\text{CaO}_2$  catalysis by  $\text{Fe}^{2+}$ , the existence of  $^1\text{O}_2$  was neglected and the mechanism of its formation remains unclear. Previous studies have shown that  $^1\text{O}_2$  formation could be well explained using molecular orbital theory. As shown in Fig. 3C, an electron in the  $\pi^*_{2p_z}$  orbital of the peroxide bond ( $\text{O}_2^{2-}$ ) was captured using a strong oxidant such as  $\cdot\text{OH}$  or  $\text{Fe}^{3+}$ , leaving a lone electron to form a superoxide free radical ( $\cdot\text{O}_2^-$ ) as described in Eq. 13 and Eq. 14 (Fig. 3C, red arrow). The lone electron on  $\pi^*_{2p_z}$  was more likely to be lost due to general chemical principles, indicating that  $\cdot\text{O}_2^-$  was more susceptible to oxidation by  $\cdot\text{OH}$  or  $\text{Fe}^{3+}$  to form  $^1\text{O}_2$ , as described by Eq. 15 and Eq. 16 (Fig. 3C, blue arrow). However,  $^1\text{O}_2$  existed in an excited state, eventually releasing energy and returning back to its ground state  $^3\text{O}_2$  (Fig. 3C, green arrow).



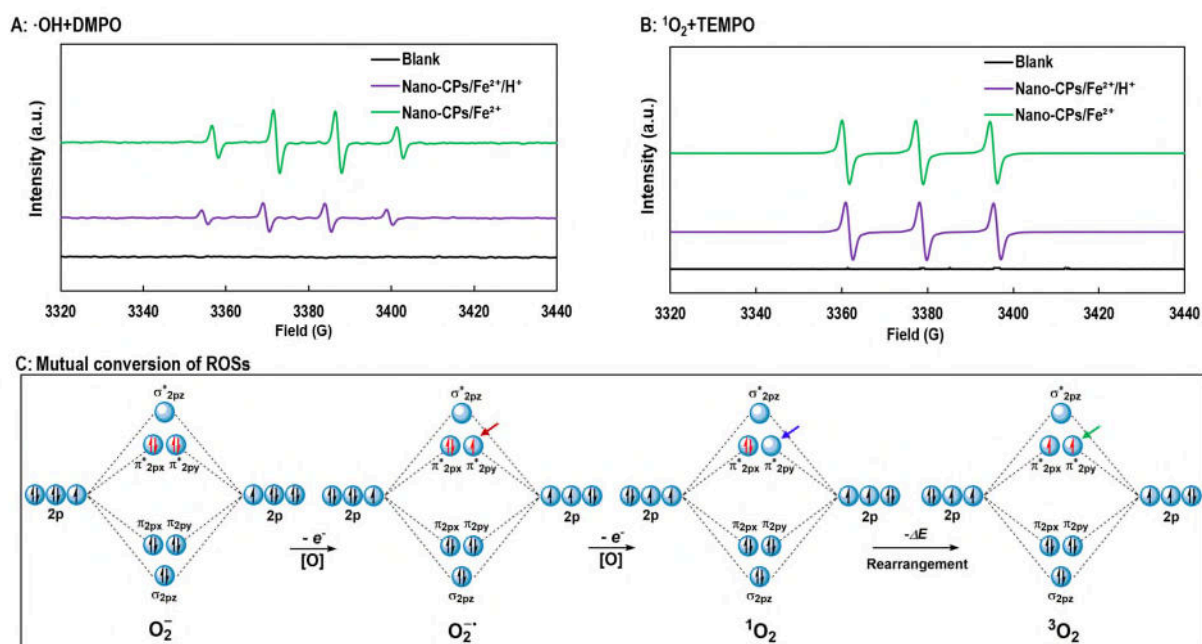


**Figure 3.** ESR diagram of  $\cdot\text{OH}$  and the  ${}^1\text{O}_2$

Previous studies had shown that both  $\cdot\text{OH}$  and  ${}^1\text{O}_2$  had high activity and can be used for the degradation of organic pollutants [47, 55-59]. Therefore, in order to establish the main species responsible for PNP degradation, methanol was added to the system as a  $\cdot\text{OH}$  quencher and  $\cdot\text{OH}$  quenching tests were carried out, as shown in Fig. 4C.  $\cdot\text{OH}$  was quenched preferentially by methanol with high reactivity ( $k_{(\text{CH}_3\text{OH}, \cdot\text{OH})} = 9.7 \times 10^8 \text{ M}^{-1}\text{s}^{-1}$  [60]), making it unable to degrade PNP, thus proving that the main factor in PNP degradation was  $\cdot\text{OH}$  originating from the Fenton process.

### 3.3.3. Cd removal

The removal mechanism of Cd was that  $\text{Ca}(\text{OH})_2$ , one of the hydrolyzates of nano- $\text{CaO}_2$ , would release  $\text{OH}^-$ , and then ferrite co-precipitation was induced to separate Cd ions from the solution in the presence of Fe agent. As a result, High pH conditions facilitated the removal of Cd (Eq. 12). As shown in Fig. 2B, at reaction times of 30, 60, 120 and 180 min, the pH increased from an initial level of 2.8 to 4.3, 5.2, 6.2, and 10.3, respectively, with corresponding Cd removal rates of 6%, 13%, 73%, and 99%. It is of note, that the concentration of Cd decreased despite consistently acidic pH conditions in the first 120 min of the reaction (Fig. 2B, green arrows). It may be speculated that Cd might be adsorbed by nano- $\text{CaO}_2$ , while Cd might also be co-precipitated by  $\text{Fe}^{2+}$  or  $\text{Fe}^{3+}$  to form ferrite [61-64].

It was worthy of note that the total amount of Cd did not decrease in the *in-situ* remediation

of groundwater, but reduced its migration and environmental risk due to the form of solid sludge. However, when the groundwater was pumped out and treated by the nano-CaO<sub>2</sub>/Fe(II), the precipitation sludge containing Cd as hazardous waste could be dewatered and desilted in the sedimentation tank.

### 3.4. Process parameters and groundwater factors

#### 3.4.1. Dose effect of the Fe(II) application

The effects of Fe<sup>2+</sup> dosage on the rates of PNP and Cd removal were investigated, as shown in Fig. 4A. Studies had shown that the PNP degradation efficiency increased significantly in accordance with increasing Fe<sup>2+</sup> dosage, whereas the rate of Cd removal decreased gradually. When Fe was not added to the reaction system, PNP degradation was minimal, while the Cd removal rate was higher. When only 5 mg of iron was added to the system, the PNP degradation rate reached 80% and the Cd removal rate reached 95% at 60 min. When the concentration of Fe was increased to above 15 mg, PNP degradation reached 93%, while the Cd removal rate reached 99% in 180 min. The PNP degradation effect was not significantly improved when an excess of Fe was added. However, the  $K_{sp}$  of Fe(OH)<sub>3</sub> ( $2.79 \times 10^{-39}$ ), Fe(OH)<sub>2</sub> ( $4.87 \times 10^{-17}$ ), and Cd(OH)<sub>2</sub> ( $7.20 \times 10^{-15}$ ) were smaller than that of Ca(OH)<sub>2</sub> ( $5.02 \times 10^{-6}$ ) at the same temperature (25 °C). It was indicated that Fe<sup>2+</sup> and Fe<sup>3+</sup> could form competitive precipitation reactions with Cd<sup>2+</sup>. Because  $K_{sp}(\text{Fe(OH)}_3) \ll K_{sp}(\text{Ca(OH)}_2)$  and  $K_{sp}(\text{Fe(OH)}_2) < K_{sp}(\text{Ca(OH)}_2)$ , Ca(OH)<sub>2</sub> would tend to react more with Fe ions (Eq. 10 and Eq. 11), which was not conducive to Cd removal due to the competitive precipitation.

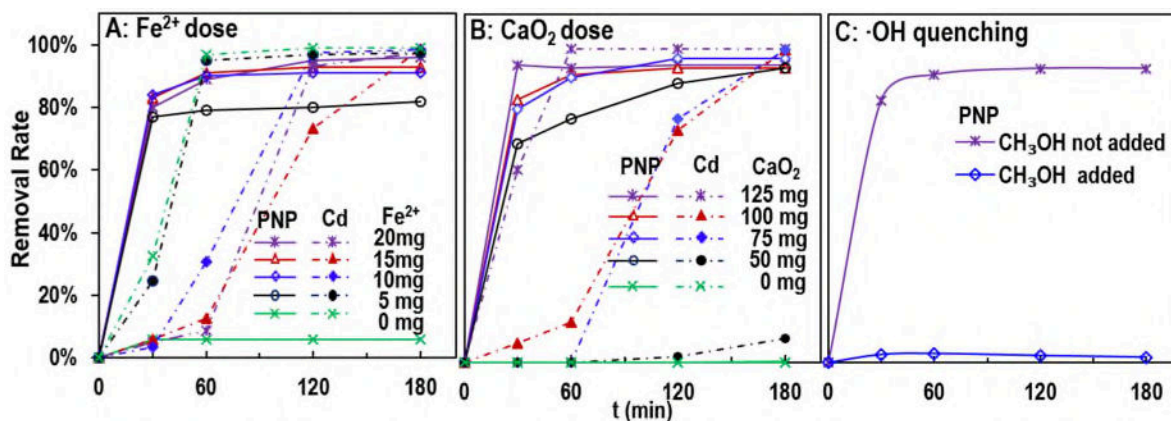
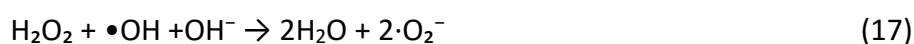


**Figure 4.** Effect of Fe<sup>2+</sup> dosage (A), CaO<sub>2</sub> dosage (B) and CH<sub>3</sub>OH quencher addition (C). The solid line represented the PNP data and the dashed line represents the Cd data. Experimental conditions: solution volume = 200 mL, initial PNP = 40 mg/L, initial Cd = 10 mg/L, Fe<sup>2+</sup> = 75 mg/L, nano-CaO<sub>2</sub> = 500 mg/L, initial pH = 2.8, oscillation frequency = 160 rpm, T = 298 K.

#### 3.4.2. Dose effect of the nano-CaO<sub>2</sub> application

The effect of different nano-CaO<sub>2</sub> dosages on PNP and Cd removal was shown in Fig. 4B. It was observed that the rates of PNP and Cd removal were both 0% without the addition of nano-

CaO<sub>2</sub>. When the dosage of nano-CaO<sub>2</sub> was 50 mg, 75 mg, 100 mg and 125 mg, the PNP degradation rates were 93%, 96%, 94% and 94%, and the Cd removal rates were 8%, 99%, 99% and 99%, respectively. The PNP degradation efficiency exhibited a trend of increasing initially and then decreasing as the nano-CaO<sub>2</sub> dosage was increased further. Actually, the system was strongly acidic and nano-CaO<sub>2</sub> was sufficient for a short period of time in the early stage. Nano-CaO<sub>2</sub>, therefore, would produce excess H<sub>2</sub>O<sub>2</sub> with H<sup>+</sup> according to Eq. 7., but the large amount of H<sub>2</sub>O<sub>2</sub> would be consumed by ·OH (Eq. 17),[\[65-67\]](#), resulting in an adverse effect on the degradation of PNP. As the high dosage of CaO<sub>2</sub> resulted in the release of more OH<sup>-</sup>, it was beneficial to the precipitation of Cd(OH)<sub>2</sub> and therefore, the rate of Cd removal was increased in accordance with the nano-CaO<sub>2</sub> dosage.



### 3.4.3. Effect of initial pH

As shown in Fig. 5, the pH value of the system was an important key factor for successful pollutant removal. High pH conditions were not conducive to the degradation of PNP, but were beneficial to the removal of Cd. In contrast, low pH conditions had an opposite effect. 93% of PNP was removed within 180 min at an initial pH of 2.8. However, when the initial pH was increased to 9.0, PNP degradation reached only 20%, while PNP degradation was negligible at an initial pH of 11.0. Because of Cd(OH)<sub>2</sub> production, it was observed that the Cd removal rate was higher under higher pH conditions. One of the reasons for the decrease in PNP removal rate was that the Fenton reaction occurred preferentially under acidic conditions. Fe<sup>3+</sup> and OH<sup>-</sup> formed Fe(OH)<sub>3</sub> precipitation under high pH conditions, causing the concentration of dissolved Fe to decrease and the catalytic degradation reaction to be interrupted, as confirmed by the variation in dissolved Fe concentrations shown in Fig. 2B. These experimental results were consistent with the conclusions of previous studies on organic pollutant degradation by Fenton processes [\[25, 68-72\]](#). In addition, low pH conditions favour the formation of H<sub>2</sub>O<sub>2</sub> from CaO<sub>2</sub> and H<sup>+</sup>, which was catalyzed to produce ·OH (Fig. 5B).

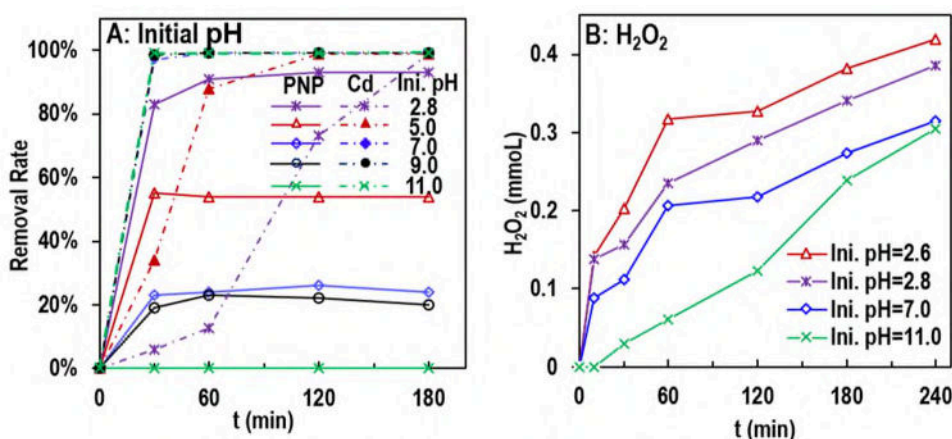


**Figure 5.** the Effect of initial pH on removal and release H<sub>2</sub>O<sub>2</sub>. (The experimental conditions: solution volume = 200 mL, oscillation frequency = 160 rpm, T = 298 K. (A) initial PNP = 40 mg/L, initial Cd = 10 mg/L, Fe<sup>2+</sup> dosage = 75 mg/mL, nano-CaO<sub>2</sub> dosage = 500 mg/mL, (B) nano-CaO<sub>2</sub> dosage = 100 mg.)

### 3.4.4. Effect of illumination, temperature and oscillation frequency

The effects of illumination, temperature and oscillation frequency on the removal of PNP and Cd by nano-CaO<sub>2</sub>/Fe (II) were shown in Fig. 6. Because the light are not the excitation condition for ·OH production catalyzed by nano-CaO<sub>2</sub>/Fe(II), exposure to light had little effect on the removal of PNP and Cd (Fig. 6A), which showed that nano-CaO<sub>2</sub>/Fe (II) was suitable for the dark environment of groundwater aquifers. As shown in Fig. 6B, low temperature conditions were not conducive to the catalytic activity of Fe<sup>2+</sup>, reducing the Fenton reaction rate and therefore, causing the PNP degradation rate to decrease [73-75]. Moreover, Low temperature would reduce the ionic activity of Cd<sup>2+</sup> and OH<sup>-</sup> and decrease their contact opportunities. Thus, the decrease in temperature was not beneficial to Cd precipitation and removal, with the time required for Cd removal rate to reach 99% reaching 180 min at 295 K, while only 60 min were required at 323 K. This illustrates that this method would require longer for the remediation of contaminated groundwater due to low groundwater temperatures.

To assess the effects of groundwater dynamics, the oscillation frequency was modified to simulate variations in water flow or water level fluctuations. As shown in Fig. 6C, within 180, the removal rates of PNP and Cd were 93% and 99% at OF=160 rpm, while the rates decreased to 78% and 32% at OF=60 rpm, respectively. It was indicated that high frequency oscillation were beneficial to the system reaction, as high frequency oscillation promoted the generation of H<sub>2</sub>O<sub>2</sub> and Ca(OH)<sub>2</sub> by CaO<sub>2</sub>, while low oscillation frequency were not conducive to the removal of PNP or Cd, which was consistent with the results of our previous study [76].

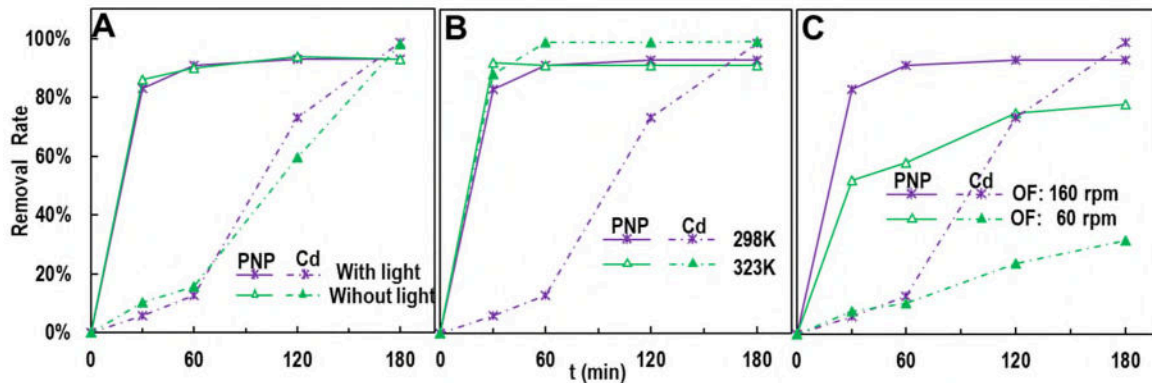


**Figure 6.** the Effect of illumination(A), temperature(B) and oscillation frequency(C). Experimental conditions: solution volume = 200 mL, initial PNP = 40 mg/L, initial Cd = 10 mg/L,  $\text{Fe}^{2+}$  dosage = 75 mg/mL, initial pH = 2.8, oscillation frequency = 160 rpm, T = 298 K.

### 3.4.5. Effect of groundwater chemical conditions

In general, the chemical composition of groundwater includes  $\text{K}^+$ ,  $\text{Na}^+$ ,  $\text{Ca}^{2+}$ ,  $\text{Mg}^{2+}$ ,  $\text{Fe}^{3+}$ ,  $\text{Mn}^{2+}$ ,  $\text{HCO}_3^-$ ,  $\text{SO}_4^{2-}$ ,  $\text{NO}_3^-$ , and  $\text{Cl}^-$  [77-79]. As shown in Fig. 7, the effects of anions and cations were studied by adding extremely high concentrations of salt to simulate real groundwater chemical characteristics to verify the applicability of the nano- $\text{CaO}_2/\text{Fe}(\text{II})$  technique in groundwater co-contaminated by PNP and Cd. Important conclusions were derived: Firstly, the addition of  $\text{Na}^+$ ,  $\text{K}^+$ ,  $\text{Ca}^{2+}$ ,  $\text{Mg}^{2+}$ ,  $\text{Fe}^{3+}$ ,  $\text{SO}_4^{2-}$ ,  $\text{Cl}^-$  and  $\text{NO}_3^-$  ions had no significant effect on PNP degradation, but the PNP degradation rate decreased from 93% to 16% after the addition of  $\text{HCO}_3^-$  (Fig. 7A, blue arrow), indicating that  $\text{HCO}_3^-$  had a negative impact on PNP removal in this system.  $\text{HCO}_3^-$  significantly affected the system pH (Eq. 18 and Eq. 19), resulting in a decrease in Fenton catalytic efficiency. Furthermore,  $\cdot\text{OH}$  was consumed in the formation of  $\text{HCO}_3^-$  from  $\text{CO}_3^{2-}$  and  $\text{OH}^-$  (Eq. 20 and Eq. 21) [25]. Results showed that  $\text{Ca}^{2+}$ ,  $\text{Mg}^{2+}$ ,  $\text{Mn}^{2+}$  and  $\text{Fe}^{3+}$  could protect the system from alkalisation (Eq. 22), reducing the system pH. Therefore, it was beneficial to the degradation of PNP and was not conducive to the removal of Cd by precipitation. However, the negative effect on Cd removal could be eliminated by increasing the nano- $\text{CaO}_2$  dosage. For example, the addition of 0.9 mM  $\text{Fe}^{3+}$  resulted in a reduction in the Cd removal rate from 99% to 24% (Fig. 7A, red arrow), However, when the nano- $\text{CaO}_2$  dosage was doubled, the removal rate returned to 99% (Fig. 7B). The PNP degradation rate reduced from 93% to 33% due to the addition of 18 mM  $\text{Mn}^{2+}$  (Fig. 7A, purple arrow), showing that PNP degradation was greatly affected by  $\text{Mn}^{2+}$ , as it could initiate a catalytic reaction to consume  $\text{H}_2\text{O}_2$  under alkaline conditions, which was not conducive to the removal of PNP. The addition of  $\text{Mn}^{2+}$  first caused the formation of  $\text{Mn}(\text{OH})_2$  using  $\text{OH}^-$  (Eq. 23), with  $\text{Mn}(\text{OH})_2$  then oxidized by  $\text{H}_2\text{O}_2$  to form black  $\text{MnO}_2$  (Eq. 24), which was consistent with experimental results with black precipitate formation. As a catalyst,  $\text{MnO}_2$  continually decomposed  $\text{H}_2\text{O}_2$  (Eq. 25) [80, 81], resulting in less  $\cdot\text{OH}$  being required to decompose PNP and ultimately causing the PNP degradation rate to be

reduced.

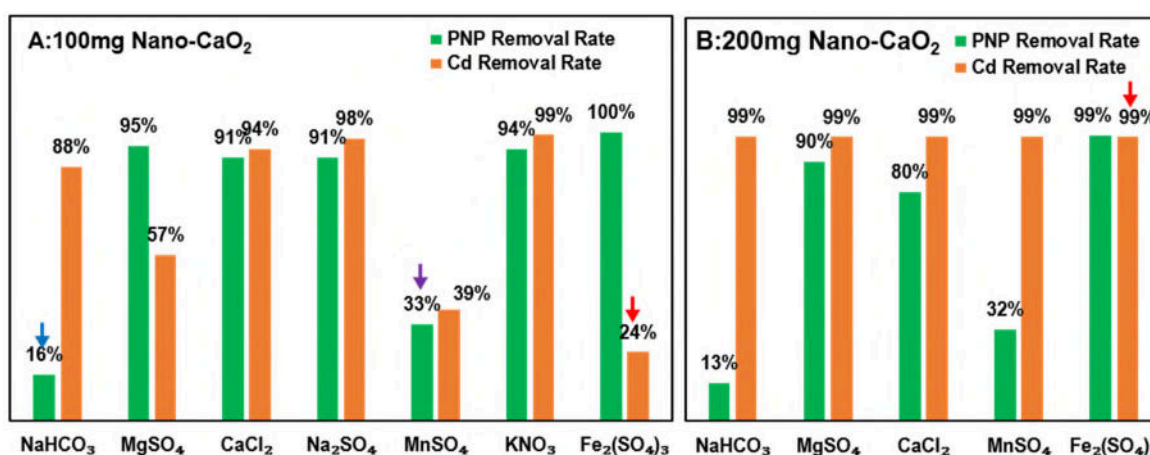
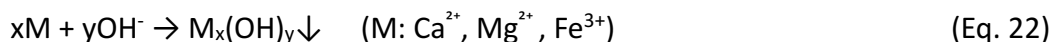


**Figure 7.** Effect of groundwater chemical composition. experimental conditions: solution volume = 200 mL, initial PNP = 40 mg/L, initial Cd = 10 mg/L, Fe<sup>2+</sup> dosage = 75 mg/mL, initial pH = 2.8, oscillation frequency = 160 rpm, T = 298 K, t = 180 min, NaHCO<sub>3</sub> = 688 mg/L, MgSO<sub>4</sub> = 996 mg/L, CaCl<sub>2</sub> = 555 mg/L, Na<sub>2</sub>SO<sub>4</sub> = 309 mg/L, KNO<sub>3</sub> = 326 mg/L, MnSO<sub>4</sub> = 272 mg/L, Fe<sub>2</sub>(SO<sub>4</sub>)<sub>3</sub> = 360 mg/L.

### 3.5. Cost evaluation of the reagents

According to the optimal reagent concentrations, it was calculated that 75 kg CaCl<sub>2</sub>, 36 kg FeSO<sub>4</sub>·7H<sub>2</sub>O, 250 L ammonia, 150 L H<sub>2</sub>O<sub>2</sub>, 500 L ethanol, and 100 L HCl would be needed to remediate 100 m<sup>3</sup> of groundwater. The total cost of reagents at current prices would be on the order of \$6680. Table S1 provided further details. Interestingly, the preparation of nano-CaO<sub>2</sub> accounted for approximately 91% of the total reagent cost. Thus, the high cost of nanopreparation would be a constraint to the development of this nano-remediation technology. Fortunately, the large amount of ammonia and ethanol (85% of material preparation cost) used in nano-CaO<sub>2</sub> preparation could be recycled, which would greatly reduce the total cost.

In addition, it is worth mentioning that the Ca salt generated as a byproduct from nano-CaO<sub>2</sub> and the Fe catalyst can be separated by precipitation without secondary pollution. More importantly, even if these green reagents are overdosed, they will not harm the environment.

So, such approach supports the sustainable development of the environment.

#### **4. Conclusion**

CaO<sub>2</sub> nanoparticles were successfully synthesized and combined with Fe<sup>2+</sup> to form a novel Fenton-like system for the treatment of combinations of the PNP and Cd. Using these nanoparticles, 93% of 40 mg/L PNP and 99% of 10 mg/L Cd were removed under the optimal conditions described. ·OH was the main factor causing PNP degradation, and the Cd removal mechanism was mainly co-precipitation with Ca(OH)<sub>2</sub> and ferrite. It was demonstrated that Low pH conditions, high Fe<sup>2+</sup> dosages, high oscillation frequencies and high temperatures were beneficial to the catalytic degradation of PNP, while high pH conditions, low Fe<sup>2+</sup> dosages, high nano-CaO<sub>2</sub> dosages, high oscillation frequencies and high temperatures were favourable for Cd precipitation and removal. In contrast, special attention should be paid to the negative effects of HCO<sub>3</sub><sup>-</sup> and Mn<sup>2+</sup> on the remediation of PNP contaminated groundwater by nano-CaO<sub>2</sub>/Fe<sup>2+</sup>, as well as to the competitive precipitation reactions of ions such as Fe<sup>3+</sup>, Ca<sup>2+</sup> and Mg<sup>2+</sup>, for the effective remediation of Cd heavy metal pollution. In conclusion, these results show that nano-CaO<sub>2</sub> based methods have high application prospects for the remediation of organic matter and heavy metals co-occurring as groundwater contaminants.

#### **CRedit authorship contributions statement**

Hui Xia conceived and performed the experiments; Hui Xia and Tao Lyu performed original draft preparation and analyzed the data; Yuesuo Yang and Chuanqi Zhao contributed reagents/materials/analysis tools, and were responsible for review and English editing; Yuesuo Yang and Jungang Guo were responsible for funding acquisition. All the authors participated in the writing and revision of the manuscript. All the authors have read and agreed to the published version of the manuscript.

#### **Acknowledgments**

This research was funded by the National Key R&D Program of China, China (2019YFC1804800); the Project Tackling of Key Scientific and Technical Problems of Henan Province, China (222102320200); the Geological Survey Program of the CGS, China (DD20221782); the Major R&D Project of Liaoning Province, China (2020JH2/10300083) and NSFC grants (Nos 42277189, 42172284)..

Acknowledgments

## References

- [1] M.M. Mekonnen, A.Y. Hoekstra, Four billion people facing severe water scarcity, *Science Advances*, 2 (2016) e1500323.
- [2] N. Moosdorf, T. Oehler, Societal use of fresh submarine groundwater discharge: An overlooked water resource, *Earth-Science Reviews*, 171 (2017) 338-348.
- [3] M. Velis, K.I. Conti, F. Biermann, Groundwater and human development: synergies and trade-offs within the context of the sustainable development goals, *Sustainability Science*, 12 (2017) 1007-1017.
- [4] L. Zhang, T. Lyu, C.A. Ramirez Vargas, C.A. Arias, P.N. Carvalho, H. Brix, New insights into the effects of support matrix on the removal of organic micro-pollutants and the microbial community in constructed wetlands, *Environmental pollution*, 240 (2018) 699-708.
- [5] J. Su, T. Lyu, H. Yi, L. Bi, G. Pan, Superior arsenate adsorption and comprehensive investigation of adsorption mechanism on novel Mn-doped  $\text{La}_2\text{O}_2\text{CO}_3$  composites, *Chemical Engineering Journal*, 391 (2020) 123623.
- [6] X. Song, Y. Zhang, N. Cao, D. Sun, L. Tao, Sustainable Chromium (VI) Removal from Contaminated Groundwater Using Nano-Magnetite-Modified Biochar via Rapid Microwave Synthesis, *Molecules*, 26 (2020) 103.
- [7] S. Jing, B. Lei, W. Chen, L. Tao, P. Gang, Enhancement of cadmium removal by oxygen-doped carbon nitride with molybdenum and sulphur hybridization, *Journal of Colloid and Interface Science*, 556 (2019).
- [8] Z.I. Bhatti, H. Toda, K. Furukawa, p-Nitrophenol degradation by activated sludge attached on nonwovens, *Water Research*, 36 (2002) 1135-1142.
- [9] H. Xia, W. Zhang, Z. Yang, Z. Dai, Y. Yang, E. Dellacassa, Spectrophotometric Determination of p-Nitrophenol under ENP Interference, *Journal of Analytical Methods in Chemistry*, 2021 (2021) 1-9.
- [10] C. Zhang, T. Li, J. Zhang, S. Yan, C. Qin, Degradation of p-nitrophenol using a ferrous-tripolyphosphate complex in the presence of oxygen: The key role of superoxide radicals, *Applied Catalysis B: Environmental*, 259 (2019) 118030.
- [11] S. Bae, S. Gim, H. Kim, K. Hanna, Effect of  $\text{NaBH}_4$  on properties of nanoscale zero-valent iron and its catalytic activity for reduction of p-nitrophenol, *Applied Catalysis B: Environmental*, 182 (2016) 541-549.
- [12] B. Lai, Z. Chen, Y. Zhou, P. Yang, J. Wang, Z. Chen, Removal of high concentration p-nitrophenol in aqueous solution by zero valent iron with ultrasonic irradiation (US-ZVI), *Journal of hazardous materials*, 250-251 (2013) 220-228.
- [13] H.K. Boparai, M. Joseph, D.M. O'Carroll, Kinetics and thermodynamics of cadmium ion removal by adsorption onto nano zerovalent iron particles, *Journal of hazardous materials*, 186 (2011) 458-465.
- [14] X. Cui, S. Fang, Y. Yao, T. Li, Q. Ni, X. Yang, Z. He, Potential mechanisms of cadmium removal from aqueous solution by *Canna indica* derived biochar, *The Science of the total environment*, 562 (2016) 517-525.
- [15] S. Rezanian, S.M. Taib, M.F. Md Din, F.A. Dahalan, H. Kamyab, Comprehensive review on phytotechnology: Heavy metals removal by diverse aquatic plants species from wastewater, *Journal of hazardous materials*, 318 (2016) 587-599.
- [16] S. Tyagi, D. Rawtani, N. Khatri, M. Tharmavaram, Strategies for Nitrate removal from aqueous

- environment using Nanotechnology: A Review, *Journal of Water Process Engineering*, 21 (2018) 84-95.
- [17] T. Zhang, G.V. Lowry, N.L. Capiro, J. Chen, W. Chen, Y. Chen, D.D. Dionysiou, D.W. Elliott, S. Ghoshal, T. Hofmann, H. Hsu-Kim, J. Hughes, C. Jiang, G. Jiang, C. Jing, M. Kavanaugh, Q. Li, S. Liu, J. Ma, B. Pan, T. Phenrat, X. Qu, X. Quan, N. Saleh, P.J. Vikesland, Q. Wang, P. Westerhoff, M.S. Wong, T. Xia, B. Xing, B. Yan, L. Zhang, D. Zhou, P.J.J. Alvarez, In situ remediation of subsurface contamination: opportunities and challenges for nanotechnology and advanced materials, *Environmental Science: Nano*, 6 (2019) 1283-1302.
- [18] X. Zhao, W. Liu, Z. Cai, B. Han, T. Qian, D. Zhao, An overview of preparation and applications of stabilized zero-valent iron nanoparticles for soil and groundwater remediation, *Water Res*, 100 (2016) 245-266.
- [19] M. Gu, U. Farooq, S. Lu, X. Zhang, Z. Qiu, Q. Sui, Degradation of trichloroethylene in aqueous solution by rGO supported nZVI catalyst under several oxic environments, *Journal of hazardous materials*, 349 (2018) 35-44.
- [20] J. Ren, Y.C. Woo, M. Yao, S. Lim, L.D. Tijing, H.K. Shon, Nanoscale zero-valent iron (nZVI) immobilization onto graphene oxide (GO)-incorporated electrospun polyvinylidene fluoride (PVDF) nanofiber membrane for groundwater remediation via gravity-driven membrane filtration, *The Science of the total environment*, 688 (2019) 787-796.
- [21] T. Wang, Y. Liu, J. Wang, X. Wang, B. Liu, Y. Wang, In-situ remediation of hexavalent chromium contaminated groundwater and saturated soil using stabilized iron sulfide nanoparticles, *Journal of environmental management*, 231 (2019) 679-686.
- [22] H. Mosmeri, F. Gholami, M. Shavandi, E. Alaie, S.M.M. Dastgheib, Application of magnesium peroxide (MgO<sub>2</sub>) nanoparticles for toluene remediation from groundwater: batch and column studies, *Environmental science and pollution research international*, 25 (2018) 31051-31061.
- [23] S. Lu, X. Zhang, Y. Xue, Application of calcium peroxide in water and soil treatment: A review, *Journal of hazardous materials*, 337 (2017) 163-177.
- [24] Y. Qian, X. Zhou, Y. Zhang, W. Zhang, J. Chen, Performance and properties of nanoscale calcium peroxide for toluene removal, *Chemosphere*, 91 (2013) 717-723.
- [25] Y. Sun, S. Lyu, M.L. Brusseau, P. Tang, W. Jiang, M. Gu, M. Li, Y. Lyu, Z. Qiu, Q. Sui, Degradation of trichloroethylene in aqueous solution by nanoscale calcium peroxide in the Fe(II)-based catalytic environments, *Separation and Purification Technology*, 226 (2019) 13-21.
- [26] Y. Liu, X. Sheng, Z. Zhou, P. Wang, Z. Lu, J. Dong, S. Lyu, Insight into Naphthalene Degradation by Nano-calcium Peroxide in Fe(II)-Citric Acid Catalytic Environment, *Water, Air, & Soil Pollution*, 232 (2021) 503.
- [27] Y. Liu, X. Sheng, Z. Zhou, P. Wang, Z. Lu, J. Dong, Y. Sun, S. Lyu, Efficient naphthalene degradation in FeS<sub>2</sub>-activated nano calcium peroxide system: Performance and mechanisms, *Journal of hazardous materials*, 432 (2022) 128693.
- [28] F. Gholami, M. Shavandi, S.M.M. Dastgheib, M.A. Amoozegar, Naphthalene remediation form groundwater by calcium peroxide (CaO<sub>2</sub>) nanoparticles in permeable reactive barrier (PRB), *Chemosphere*, 212 (2018) 105-113.
- [29] J. Khodaveisi, H. Banejad, A. Afkhami, E. Olyaie, S. Lashgari, R. Dashti, Synthesis of calcium peroxide nanoparticles as an innovative reagent for in situ chemical oxidation, *Journal of hazardous materials*, 192 (2011) 1437-1440.
- [30] X. Li, Y. Xie, F. Jiang, B. Wang, Q. Hu, Y. Tang, T. Luo, T. Wu, Enhanced phosphate removal from aqueous solution using resourceable nano-CaO<sub>2</sub>/BC composite: Behaviors and mechanisms, *The*

Science of the total environment, 709 (2020) 136123.

[31] B.S. De, K.L. Wasewar, V.R. Dhongde, P.B. Sontakke, Recovery of Acrylic Acid Using Calcium Peroxide Nanoparticles: Thermodynamics and Continuous Column Study, *Chemical and Biochemical Engineering Quarterly*, 32 (2018) 19-28.

[32] S.S. Madan, K.L. Wasewar, C.R. Kumar, Optimization of adsorptive removal of  $\alpha$ -toluic acid by  $\text{CaO}_2$  nanoparticles using response surface methodology, *Resource-Efficient Technologies*, 3 (2017) 329-336.

[33] S.S. Madan, K.L. Wasewar, Optimization for benzeneacetic acid removal from aqueous solution using  $\text{CaO}_2$  nanoparticles based on Taguchi method, *Journal of Applied Research and Technology*, 15 (2017) 332-339.

[34] S.S. Madan, K.L. Wasewar, C. Ravi Kumar, Adsorption kinetics, thermodynamics, and equilibrium of  $\alpha$ -toluic acid onto calcium peroxide nanoparticles, *Advanced Powder Technology*, 27 (2016) 2112-2120.

[35] E. Olyaie, H. Banejad, A. Afkhami, A. Rahmani, J. Khodaveisi, Development of a cost-effective technique to remove the arsenic contamination from aqueous solutions by calcium peroxide nanoparticles, *Separation and Purification Technology*, 95 (2012) 10-15.

[36] Y.Y. Jiang, Z.W. Chen, M.M. Li, Q.H. Xiang, X.X. Wang, H.F. Miao, W.Q. Ruan, Degradation of diclofenac sodium using Fenton-like technology based on nano-calcium peroxide, *The Science of the total environment*, 773 (2021) 144801.

[37] M. Ali, M. Danish, M. Tariq, A. Ahmad, K. Shahzad Ayub, S. Lyu, Mechanistic insights into the degradation of trichloroethylene by controlled release nano calcium peroxide activated by iron species coupled with nano iron sulfide, *Chemical Engineering Journal*, 399 (2020) 125754.

[38] H. Mosmeri, F. Gholami, M. Shavandi, S.M.M. Dastgheib, E. Alaie, Bioremediation of benzene-contaminated groundwater by calcium peroxide ( $\text{CaO}_2$ ) nanoparticles: Continuous-flow and biodiversity studies, *Journal of hazardous materials*, 371 (2019) 183-190.

[39] H. Mosmeri, E. Alaie, M. Shavandi, S.M.M. Dastgheib, S. Tasharrofi, Benzene-contaminated groundwater remediation using calcium peroxide nanoparticles: synthesis and process optimization, *Environmental Monitoring and Assessment* 189 (2017) 452.

[40] P. Kaewdee, N. Chandet, G. Rujijanagul, C. Randorn, Multicatalytic properties of nanoparticle  $\text{CaO}_2$  synthesized by a novel, simple and economical method for wastewater treatment, *Catalysis Communications*, 84 (2016) 151-154.

[41] C.S. Yeh, R. Wang, W.C. Chang, Y.H. Shih, Synthesis and characterization of stabilized oxygen-releasing  $\text{CaO}_2$  nanoparticles for bioremediation, *Journal of environmental management*, 212 (2018) 17-22.

[42] H.H. Eysel, S. Thym, RAMAN Spectra of Peroxides, *Zeitschrift für anorganische und allgemeine Chemie*, 411 (1975) 97-102.

[43] K. Zhou, B. Wu, L. Su, X. Gao, X. Chai, X. Dai, Development of nano- $\text{CaO}_2$ -coated clinoptilolite for enhanced phosphorus adsorption and simultaneous removal of COD and nitrogen from sewage, *Chemical Engineering Journal*, 328 (2017) 35-43.

[44] B. Wu, L. Su, X. Dai, X. Chai, Development of montmorillonite-supported nano  $\text{CaO}_2$  for enhanced dewatering of waste-activated sludge by synergistic effects of filtration aid and peroxidation, *Chemical Engineering Journal*, 307 (2017) 418-426.

[45] B.S. De, Recovery of Acrylic Acid Using Calcium Peroxide Nanoparticles: Synthesis, Characterisation, Batch Study, Equilibrium, and Kinetics, *Chemical and Biochemical Engineering Quarterly*, 32 (2018) 29-39.

- [46] H. Mosmeri, E. Alaie, M. Shavandi, S.M.M. Dastgheib, S. Tasharrofi, Bioremediation of benzene from groundwater by calcium peroxide (CaO<sub>2</sub>) nanoparticles encapsulated in sodium alginate, *Journal of the Taiwan Institute of Chemical Engineers*, 78 (2017) 299-306.
- [47] M. Cheng, G. Zeng, D. Huang, C. Lai, P. Xu, C. Zhang, Y. Liu, Hydroxyl radicals based advanced oxidation processes (AOPs) for remediation of soils contaminated with organic compounds: A review, *Chemical Engineering Journal*, 284 (2016) 582-598.
- [48] T.A. Kurniawan, G.Y.S. Chan, W.-H. Lo, S. Babel, Physico-chemical treatment techniques for wastewater laden with heavy metals, *Chemical Engineering Journal*, 118 (2006) 83-98.
- [49] A. Azimi, A. Azari, M. Rezakazemi, M. Ansarpour, Removal of Heavy Metals from Industrial Wastewaters: A Review, *ChemBioEng Rev.*, 4 (2017) 37-59.
- [50] M. Munoz, Z.M. de Pedro, J.A. Casas, J.J. Rodriguez, Preparation of magnetite-based catalysts and their application in heterogeneous Fenton oxidation – A review, *Applied Catalysis B: Environmental*, 176-177 (2015) 249-265.
- [51] J. Zhao, N. Liu, S. Sun, S. Gou, X. Wang, Z. Wang, X. Li, W. Zhang, Light-activated ruthenium (II)-bicalutamide prodrugs for prostate cancer, *Journal of Inorganic Biochemistry*, 196 (2019) 110684.
- [52] C.S.D. Rodrigues, O.S.G.P. Soares, M.T. Pinho, M.F.R. Pereira, L.M. Madeira, p-Nitrophenol degradation by heterogeneous Fenton's oxidation over activated carbon-based catalysts, *Applied Catalysis B: Environmental*, 219 (2017) 109-122.
- [53] J.M. Fontmorin, R.C. Burgos Castillo, W.Z. Tang, M. Sillanpaa, Stability of 5,5-dimethyl-1-pyrroline-N-oxide as a spin-trap for quantification of hydroxyl radicals in processes based on Fenton reaction, *Water Res*, 99 (2016) 24-32.
- [54] J. Wandt, P. Jakes, J. Granwehr, H.A. Gasteiger, R.-A. Eichel, Singlet Oxygen Formation during the Charging Process of an Aprotic Lithium-Oxygen Battery, *Angewandte Chemie International Edition*, 55 (2016) 6892-6895.
- [55] D.B. Miklos, C. Remy, M. Jekel, K.G. Linden, J.E. Drewes, U. Hubner, Evaluation of advanced oxidation processes for water and wastewater treatment - A critical review, *Water Res*, 139 (2018) 118-131.
- [56] S. Gligorovski, R. Streckowski, S. Barbat, D. Vione, Environmental Implications of Hydroxyl Radicals (•OH), *Chemical Reviews*, 115 (2015) 13051-13092.
- [57] H. Yi, D. Huang, L. Qin, G. Zeng, C. Lai, M. Cheng, S. Ye, B. Song, X. Ren, X. Guo, Selective prepared carbon nanomaterials for advanced photocatalytic application in environmental pollutant treatment and hydrogen production, *Applied Catalysis B: Environmental*, 239 (2018) 408-424.
- [58] P. Liang, C. Zhang, X. Duan, H. Sun, S. Liu, M.O. Tade, S. Wang, An insight into metal organic framework derived N-doped graphene for the oxidative degradation of persistent contaminants: formation mechanism and generation of singlet oxygen from peroxydisulfate, *Environmental Science: Nano*, 4 (2017) 315-324.
- [59] M. Cao, R. Pang, Q.-Y. Wang, Z. Han, Z.-Y. Wang, X.-Y. Dong, S.-F. Li, S.-Q. Zang, T.C.W. Mak, Porphyrinic Silver Cluster Assembled Material for Simultaneous Capture and Photocatalysis of Mustard-Gas Simulant, *Journal of the American Chemical Society*, 141 (2019) 14505-14509.
- [60] S. Zhu, X. Li, J. Kang, X. Duan, S. Wang, Persulfate Activation on Crystallographic Manganese Oxides: Mechanism of Singlet Oxygen Evolution for Nonradical Selective Degradation of Aqueous Contaminants, *Environmental science & technology*, 53 (2019) 307-315.
- [61] M. Kaur, N. Kaur, Vibha, Ferrites: Synthesis and Applications for Environmental Remediation, in: *Ferrites and Ferrates: Chemistry and Applications in Sustainable Energy and Environmental*

Remediation, American Chemical Society, 2016, pp. 113-136.

[62] F. Liu, K. Zhou, Q. Chen, A. Wang, W. Chen, Comparative study on the synthesis of magnetic ferrite adsorbent for the removal of Cd(II) from wastewater, *Adsorption Science & Technology*, 36 (2018) 1456-1469.

[63] K.K. Kefeni, B.B. Mamba, T.A.M. Msagati, Application of spinel ferrite nanoparticles in water and wastewater treatment: A review, *Separation and Purification Technology*, 188 (2017) 399-422.

[64] I. Ali, New Generation Adsorbents for Water Treatment, *Chemical Reviews*, 112 (2012) 5073-5091.

[65] A. Fischbacher, C. von Sonntag, T.C. Schmidt, Hydroxyl radical yields in the Fenton process under various pH, ligand concentrations and hydrogen peroxide/Fe(II) ratios, *Chemosphere*, 182 (2017) 738-744.

[66] R.J. Watts, A.L. Teel, Hydroxyl radical and non-hydroxyl radical pathways for trichloroethylene and perchloroethylene degradation in catalyzed H<sub>2</sub>O<sub>2</sub> propagation systems, *Water Res*, 159 (2019) 46-54.

[67] F. Chen, S. Xie, X. Huang, X. Qiu, Ionothermal synthesis of Fe<sub>3</sub>O<sub>4</sub> magnetic nanoparticles as efficient heterogeneous Fenton-like catalysts for degradation of organic pollutants with H<sub>2</sub>O<sub>2</sub>, *Journal of hazardous materials*, 322 (2017) 152-162.

[68] L. Chu, J. Wang, J. Dong, H. Liu, X. Sun, Treatment of coking wastewater by an advanced Fenton oxidation process using iron powder and hydrogen peroxide, *Chemosphere*, 86 (2012) 409-414.

[69] X. Qian, M. Ren, M. Fang, M. Kan, D. Yue, Z. Bian, H. Li, J. Jia, Y. Zhao, Hydrophilic mesoporous carbon as iron(III)/(II) electron shuttle for visible light enhanced Fenton-like degradation of organic pollutants, *Applied Catalysis B: Environmental*, 231 (2018) 108-114.

[70] S. Li, G. Zhang, P. Wang, H. Zheng, Y. Zheng, Microwave-enhanced Mn-Fenton process for the removal of BPA in water, *Chemical Engineering Journal*, 294 (2016) 371-379.

[71] H. Che, S. Bae, W. Lee, Degradation of trichloroethylene by Fenton reaction in pyrite suspension, *Journal of hazardous materials*, 185 (2011) 1355-1361.

[72] J. Cao, Z. Xiong, B. Lai, Effect of initial pH on the tetracycline (TC) removal by zero-valent iron: Adsorption, oxidation and reduction, *Chemical Engineering Journal*, 343 (2018) 492-499.

[73] J.A. Sánchez Pérez, P. Soriano-Molina, G. Rivas, J.L. García Sánchez, J.L. Casas López, J.M. Fernández Sevilla, Effect of temperature and photon absorption on the kinetics of micropollutant removal by solar photo-Fenton in raceway pond reactors, *Chemical Engineering Journal*, 310 (2017) 464-472.

[74] N. Ertugay, F.N. Acar, Removal of COD and color from Direct Blue 71 azo dye wastewater by Fenton's oxidation: Kinetic study, *Arabian Journal of Chemistry*, 10 (2017) S1158-S1163.

[75] Y. Yao, H. Chen, J. Qin, G. Wu, C. Lian, J. Zhang, S. Wang, Iron encapsulated in boron and nitrogen codoped carbon nanotubes as synergistic catalysts for Fenton-like reaction, *Water Res*, 101 (2016) 281-291.

[76] H. Xia, J. Guo, Y. Yang, Y. Wang, Z. Wang, X. Wang, W. Zhang, Remediation of PNP-contaminated groundwater using a modified CaO<sub>2</sub>/Fe(II) Fenton system: Reactive principles, degradation performance and potential pathways, *Journal of Environmental Chemical Engineering*, 10 (2022) 107305.

[77] P. Liu, N. Hoth, C. Drebenstedt, Y. Sun, Z. Xu, Hydro-geochemical paths of multi-layer groundwater system in coal mining regions - Using multivariate statistics and geochemical modeling approaches, *The Science of the total environment*, 601-602 (2017) 1-14.

[78] Y. Jia, B. Xi, Y. Jiang, H. Guo, Y. Yang, X. Lian, S. Han, Distribution, formation and human-induced evolution of geogenic contaminated groundwater in China: A review, *The Science of the total environment*, 643 (2018) 967-993.

- [79] D. Jellalia, F. Lachaal, M. Andoulsi, T. Zouaghi, M. Hamdi, M. Bedir, Hydro-geophysical and geochemical investigation of shallow and deep Neogene aquifer systems in Hajeb Layoun-Jilma-Ouled Asker area, Central Tunisia, *Journal of African Earth Sciences*, 110 (2015) 227-244.
- [80] A. Izgorodin, E. Izgorodina, D.R. MacFarlane, Low overpotential water oxidation to hydrogen peroxide on a MnOx catalyst, *Energy & Environmental Science*, 5 (2012) 9496.
- [81] A.L. Pham, F.M. Doyle, D.L. Sedlak, Inhibitory effect of dissolved silica on H<sub>2</sub>O<sub>2</sub> decomposition by iron(III) and manganese(IV) oxides: implications for H<sub>2</sub>O<sub>2</sub>-based in situ chemical oxidation, *Environmental science & technology*, 46 (2012) 1055-1062.

# ***Supporting Information for***

## **Synergistic removal of organic micropollutants and inorganic heavy metals by nano-calcium peroxide induced Fenton-like treatment**

**Hui Xia<sup>a,b</sup>, Tao Lyu<sup>c</sup>, Jungang Guo<sup>a,b\*</sup>, Chuanqi Zhao<sup>d\*</sup>, Yuesuo Yang<sup>e\*</sup>**

<sup>a</sup> Zhengzhou Institute of Multipurpose Utilization of Mineral Resources, CAGS, Zhengzhou 450006, China;

<sup>b</sup> China National Engineering Research Center for Utilization of Industrial Minerals, Zhengzhou 450006, China;

<sup>c</sup> School of Water, Energy and Environment, Cranfield University, College Road, Cranfield, Bedfordshire, MK43 0AL, United Kingdom;

<sup>d</sup> School of Materials and Environment, Guangxi University for Nationalities, Nanning 530006, China;

<sup>e</sup> Key Lab of Groundwater Resources and Environment (Jilin University), Ministry of Education, Changchun 130021, China.

### **Contents**

Supporting document. 1-Analytical methods .....	2
1.1 Analytical method of H <sub>2</sub> O <sub>2</sub> .....	2
1.2 Analytical method of CaO <sub>2</sub> .....	2
1.3 Qualitative analytical method of ROS. ....	2
Supporting document. 2-Figures .....	2
Figure S1. Chemical structure of CaO <sub>2</sub> .....	2
Figure S2. TEM of CaO <sub>2</sub> .....	2
<b>References</b> .....	<b>2</b>

## 1 Supporting document. 1-Analytical methods

### 2 1.1 Analytical method of H<sub>2</sub>O<sub>2</sub>

3 The measurement of H<sub>2</sub>O<sub>2</sub> was carried out by spectrophotometry[1, 2]. The brief steps were: adding  
4 1.00mL sample, 2mL 2.5 mM ammonium molybdate and 2mL 0.5 M sulfuric acid in 5mL water, and  
5 measuring at 340nm after 15min.

### 6 1.2 Analytical method of CaO<sub>2</sub>

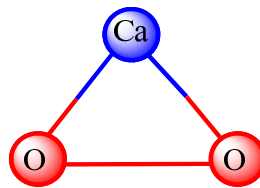
7 CaO<sub>2</sub> was measured by potassium permanganate titration. The potassium permanganate solution  
8 calibrated by oxalic acid was used to titrate the content of H<sub>2</sub>O<sub>2</sub> which was generated by CaO<sub>2</sub> under  
9 strong acid conditions. The color of the titration end point was pink.

### 10 1.3 Qualitative analytical method of ROS

11 200mg/L DMPO capture agent or TEMPO capture agent was added to the sample in advance, and  
12 then the quantitative FeSO<sub>4</sub> and CaO<sub>2</sub> solution were added. ESR was immediately scanned after 5  
13 minutes of reaction.

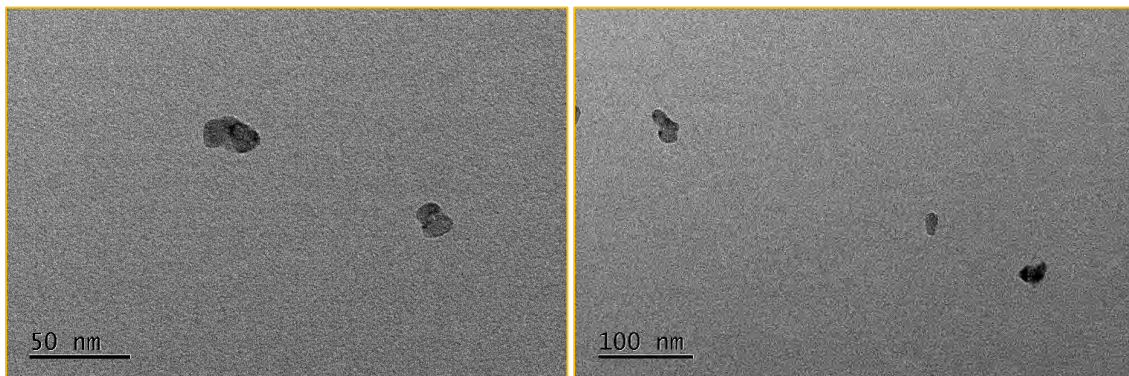
## 14 Supporting document. 2- Figure

15 Figure S1. Chemical structure of CaO<sub>2</sub>



16

17 Figure S2. TEM of CaO<sub>2</sub>



18

## 19 References

- 20 [1] X.S. Chai, Q.X. Hou, Q. Luo, J.Y. Zhu, Rapid determination of hydrogen peroxide in the wood pulp  
21 bleaching streams by a dual-wavelength spectroscopic method, *Anal. Chim. Acta*, 507 (2004) 281-284.  
22 [2] H. Wang, Y. Zhao, T. Li, Z. Chen, Y. Wang, C. Qin, Properties of calcium peroxide for release of  
23 hydrogen peroxide and oxygen: A kinetics study, *Chem. Eng. J.*, 303 (2016) 450-457.

24

# Simultaneous removal of organic micropollutants and inorganic heavy metals by nano-calcium peroxide induced Fenton-like treatment

Xia, Hui

2022-11-01

Attribution-NonCommercial-NoDerivatives 4.0 International

---

Xia H, Lyu T, Guo J, et al., (2023) Simultaneous removal of organic micropollutants and inorganic heavy metals by nano-calcium peroxide induced Fenton-like treatment. *Separation and Purification Technology*, Volume 305, January 2023, Article number 122474

<https://doi.org/10.1016/j.seppur.2022.122474>

*Downloaded from CERES Research Repository, Cranfield University*